LAWRENCE
LIVERMORE
NATIONAL
LABORATORY

LLNL-CONF-654798

Carbon ion flow measurements in DIII-D divertors by coherence imaging

S. L. Allen, W. H. Meyer, G. D. Porter, J. Howard

May 22, 2014

21st Plasma Surface Interactions Meeting
Kanazawa, Japan
May 25, 2014 through May 30, 2014

Disclaimer

Carbon ion flow measurements in DIII-D divertors by coherence imaging*

S.L. Allen[1], W.H. Meyer[1], G.D. Porter[1], and J. Howard[2]

[1]*Lawrence Livermore National Laboratory, Livermore, CA 94550, USA*

[2]*Australia National University, Canberra, ACT 02000, Australia*

Abstract

Coherence Imaging Spectroscopy (CIS) obtains an interferogram image of plasma impurity emissions at a fixed optical delay. For the results presented here, the CIS optical delay is chosen so that the phase of the interferogram is related to the Doppler shift of CIII emissions at 465nm. Recent results from a new side-lab calibration technique agree well with previous model-based calculations of the relationship between CIS phase and wavelength. Data from both the lower and upper divertor systems has been obtained during a wide variety of operating conditions, including lower single null (LSN) and double null (DN) discharges in L- and H-mode. For the upcoming DIII-D run campaign, precise temperature regulation of the CIS along with a new in-situ calibration system has been installed so that absolute velocity measurements should be possible; previously it was assumed that the flow velocity was ~0 during the plasma breakdown phase.

Abstract length (150 words): 147 currently

PACS: 52.30.-q, 52.40.Hf, 52.55.Fa, 52.25.Rk
PSI-20 keywords: Plasma Flow, DIII-D, Divertor diagnostic, Spectroscopy, Visible Imaging
**Corresponding author address: General Atomics, 3550 General Atomics Court, San Diego, CA 92121*
**Corresponding author E-mail: allens@fusion.gat.com*

1. Introduction

The flow of plasma and impurities in the Scrape-Off-Layer (SOL) and divertor determines the impurity density and radiation profiles in these regions, which in turn influences the heat flux incident on the divertor plate ("radiative divertor"), the quality of the core plasma (confinement and dilution), and the location of eroded and deposited plasma wall materials. From the Braginskii equations [1], we expect interplay between the main ion, electron, and impurity transport; particularly by way of the predicted frictional and thermal forces on the impurities.

Mach probes have been used extensively in the SOL to measure main ion flows and temperatures on several tokamaks [2]; these measurements are often restricted to lower power plasmas such as L-mode to ensure survivability of the probes. Bulk impurity flows have been inferred from injecting a tracer impurity such as ^{13}C[3], followed by removal and analysis of in-vessel tiles. A general observation is that (carbon) impurities are transported to the inner divertor strike point; this trend is less clear in ELMing plasmas. Impurity flow velocities have also been directly measured at several discrete locations in the SOL with "conventional" high resolution spectroscopy [4]. As these are usually measurements integrated along a chord of the tokamak, the emission line profiles are the superposition of shifted Gaussians, with the assumption that the ion temperature is constant. This requires careful fitting of the chord-averaged emission profiles, and can include the use of additional spectral information such as the Zeeman splitting to help localize the location of the emission [5].

A different measurement approach is to use Fourier Transform interferometric techniques; in this case the change in the width and the shift in the central wavelength of the emission line or multiplet can be separately examined. In the general case, a Michelson interferometer is scanned through a range of delays and the resulting interferogram can be

used to reconstruct a high resolution spectrum. Depending on the resolution required, the scan could take tens of ms up to several minutes, thereby limiting the time resolution of the measurement. In the field of plasma physics, Howard has pioneered a technique using an interferogram image at a fixed delay; this delay is chosen so that either the interferogram phase is sensitive (primarily) to the change in the central wavelength (Doppler shift used for flow velocity – the case for this study), or the contrast of the interferogram is (primarily) sensitive to the change in width (Doppler width used for ion temperature) [6]. The two-arm Michelson interferometer is realized in a compact form factor with a birefringent crystal, which has a different index of refraction (and hence a difference in optical path length) for each of the two orthogonal states of polarization. Early work used a separate "displacer" crystal (analogous to the beam splitter in the Michelson) and a "delay" crystal (analogous to the optical path difference of the two arms in the Michelson) to produce the interferogram. The current work uses a single crystal cut at a specific angle to provide both the displacement and the optical path delay. The equations for the optical delay from a uniaxial crystal plate cut obliquely to the optic axis are given in Ref. 7. The CIS is simple and compact: a birefringent crystal between a pair of crossed polarizers; a collimating lens provides a parallel beam path through the CIS and a 465 nm (3 mn) interference filter, followed by a focusing lens, which images the interferogram on the camera sensor.

Previous work [8] on DIII-D generated an interferogram image of CIII emissions in the DIII-D lower divertor during the steady-state phase of an L-mode discharge. The FFT-computed phase image of the interferogram was then inverted to obtain a 2-D distribution of C2+ flow; the ion flow was from the x-point to the plate at the outer divertor, and in the opposite sense in the private flux region and in a zone above the x-point at the inner divertor. (The inner divertor was detached, so there was very little CIII emission between the x-point

and inner strike point due to the low plasma temperature). These measurements were compared with UEDGE fluid code simulations and good agreement was found in the overall structure.

2. Improvements and Additions to the DIII-D CIS system

Since these first measurements, several improvements to the (CIS) system in the lower divertor have been implemented, a new system was installed in the upper divertor, and a wide-angle periscope system viewing the whole plasma cross section is being constructed. In the DIII-D neutron environment, the camera is housed in a triple shield, located ~2 m away from the tokamak: borated polyethylene (neutrons), lead (gamma- and x-rays), and iron (magnetic shielding). A periscope inside DIII-D relays the divertor light to a real image at the exit of the tokamak port; this was transferred to the CIS and camera with a coherent fiber bundle. The transmission of this bundle at the CIII wavelength (465 nm) is ~30% for a new fiber, and degrades (~1 month) with neutron flux. Replacing this with a telescope and mirrors, along with custom high-transmission (90%) filters from Alluxa, has significantly increased the temporal (~1 ms from 20 ms) and spatial resolution (~few mm) of the system so that ELM events can be measured. Data for the DIII-D 2013 campaign used this new optical system, and one type of rapid intershot processing is shown in Fig. 2 for a demonstration shot; the three colored boxes are selected by the user, and then the line-integrated time histories of the phase (proportional to line-integrated Doppler shift and thereby line-integrated velocity) are computed. The shape changes from nearly diverted to circular, and the three regions have corresponding changes in the phase.

3. Calibration of the CIS system; in-situ calibration on DIII-D for Lower Divertor

There were three main contributions to the error bars of the previous measurements: 1) the first visible frame of the plasma was assumed to be the phase image corresponding to a

zero velocity or “rest frame wavelength” of the CIII multiplet, 2) the temperature regulation of the CIS crystal was not precise enough to determine if the velocity of the first frame was changing with different plasma conditions, and 3) the sensitivity of the phase with wavelength was determined from equations [7] using the index of refraction of the particular crystal along with the crystal geometry (supplied by the manufacturer). In general, a Zn lamp with a bright line at 468 nm was used (with a different filter centered at this wavelength) to obtain the shape of the phase image, and then this shape was translated in phase to correspond to the zero velocity at the beginning of the discharge.

As temperature control was a prerequisite to obtaining stable calibration images, two approaches were used: sensitive feedback control of the crystal temperature, and replacing the LiNBO3 crystals with alpha-BBO, which are expected to have significantly less change in birefringence with temperature. Previously, a commercial filter oven was used to control the temperature of the CIS to ≤ 1 degree C. The improved system mounts the crystal and two polarizers in symmetric aluminum rotation mounts; aluminum was used to minimize thermal gradients. Four small heater elements are attached to the CIS mount, and a thermistor is mounted in direct contact with the crystal. This assembly is thermally isolated from the rest of the optics and is surrounded with 100mm of insulation. A Proportional-Integral feedback loop with high gain controls the heater (only 2-3 Watts are required); the measured stability is ±0.02 degrees C. This system was also used to measure the temperature sensitivity of the system; for a 5.8mm alpha-BBO crystal cut at 60 degrees, the measured change in phase was ~0.078 radians per degree C. With temperature regulation, the expected drift would be ~±.0016 radians.

The CIS calibration is analogous to the a) dispersion calibration and b) absolute wavelength calibration of a conventional spectrometer: the relationship between the a) CIS

change in phase and the change in wavelength is required to measure *changes* in velocity, and the b) change in phase relative to a fixed wavelength is required to measure the "absolute" velocity relative to a reference frame. The sensitivity (a), as discussed above, is modeled by the equations of Ref. 7, knowing the crystal angle and thickness, and the extraordinary and ordinary indices of refraction. Due to the long history of plasma measurements with CIS, good agreement with the model was expected. Previous measurements with a tuneable dye laser [9] also showed good agreement with the model. The current work extends the wavelength range of the comparison with the model, and also shows good agreement. The NIST wavelength tables were used to locate emission lines in the region of 465 nm, and the intensity of these lines was examined experimentally in several light sources. Hollow cathode emission lamps, available commercially for Atomic Absorption spectroscopy, offer very narrow emission lines with long coherence lengths, but it is difficult to predict the relative brightness of lines, and in general they are significantly less bright and smaller in size than the (ideal) Zn lamp at 468 nm. As shown in Fig. 3, a search of about twelve elements yielded several lines: Cu 4651.12 Å, Ti 4656.4693 Å, Eu 4661.888 Å, Ti 4667.4 Å, Ti 4681.908, and Zn 4680.14 Å; the NIST wavelengths are shown, but the locations were verified with a high resolution spectrometer. From the model, it was expected that this particular crystal (alpha-BBO 5.8 mm, 30 degree cut angle our label Claser1) would have more than one fringe (change in phase by 2π) for the ~5 Å separation between the lines. Therefore, a 4651.2 Å (room temperature) 1.5 Å interference filter with a white light source was thermally tuned to obtain a range of low coherence wavelengths up to 4653.7 Å. The coherence (amplitude of the interferogram) was greatly reduced for this source, but it was easily demodulated to obtain the slope of the overall curve. A mirror was used to direct the filtered light to a high resolution spectrometer at each measurement point (filter temperature) to measure the relative

change in wavelength. These points are plotted with the + symbols in Fig. 3 and provide a rough slope of the sensitivity.

Interferograms were then obtained for each of the sources: Cu, Ti, Eu, Ti, and Zn; these were then demodulated (i.e. the carrier removed by Fourier Transform) and the resulting phase images were subtracted to yield the phase difference. An average of pixels near the center of the (PCO-16) 1600 by 1200 pixel image was used for the data in Fig. 3. In general, the phase difference images were very flat, indicating a difference of two monochromatic sources, with a slight slope from top to bottom (the fringes are horizontal in the image). Two interference filters mounted in a motorized filter wheel were required to obtain the plot; one centered at 4650 Å used for the CIII plasma images, and a second at 4686.4 Å used for the Zn lamp. The filters did not overlap (transmit) in the region of the 4667.4 Å Ti line, allowing it to be isolated, so that only one Ti line was transmitted by the either the 4650Å or 4686.4 Å filter. The slope of the (emission line) curve in Figure 3 yields the sensitivity of this particular CIS, $(\Delta\varphi/2\pi) = 1350 \pm 21\ (\Delta\lambda/\lambda)$, and substituting for the Doppler shift, $(\Delta\varphi/2\pi) = 1350\ (v/c)$, resulting in $v \approx 35\ \Delta\varphi$ km s^{-1}, and a one radian change in phase would correspond to a Doppler shift velocity of 35 km s^{-1}. From the model [7], using the published index of refraction for *beta*-BBO, the mean calculated delay is 1353 waves, which agrees well with the experimental result. Thus, we can expect the model to be a good predictor for other crystals, and the sensitivity is consistent with the specified crystal geometry. For the PCO.1600 camera and this crystal, one fringe corresponded to ~14 pixels. The lower divertor Phantom 7.3 camera has lower resolution (800 by 600 pixels), so a different crystal (alpha-BBO, 5mm, 75 degrees) was used with a calculated mean delay of 1418 waves, and ~10 pixels per fringe.

This same side-lab calibration technique was then implemented in the lower divertor of DIII-D; only a Ti hollow cathode and the Zn lamp were used. The geometry of the calibration source was designed to be as close to that of the plasma, with the limitation that the intensity of the calibration sources are much less than the plasma CIII emissions. The Ti lamp provides a reference wavelength that transmits through the same filter as that used for the CIII plasma emissions – i.e. no changes in the optics. The Zn lamp provides a brighter, more uniform source, necessitating a change in the filter. While it is desirable to use a diffusing medium such as an integrating sphere with the lamp sources, the corresponding reduction in intensity – particularly for the hollow cathode source – makes this impractical, so no diffusion was used. A pneumatically driven mirror directs the light from the calibration source into the front lens of the system, a second mirror can select either source, and the filters are changed with a motorized filter wheel. The system is currently operational in the DIII-D experimental hall and the wavelength stability of the system is being assessed at the start of the 2014 experimental campaign.

4. Future work

A detailed physics description of carbon flows from the data is beyond the scope of the present discussion. While the data from the 2013 campaign is not temperature compensated, it is being analyzed for trends, such as basic changes with forward and reverse toroidal field. Recall that the sensitivity of the crystal is well known, so that measurements of the *change* in flow are valid, it is the "rest" wavelength or zero velocity that must be estimated. Also, computation of *changes* in flow can (independently) cover any part of the discharge; i.e. it is the relative phase change that is important.

A new calibration technique, coupled with addition of precision temperature control of the crystal optics has reduced the absolute velocity uncertainty to an estimated ~2 km/s;

detailed stability measurements are in progress as this system has been installed on DIII-D. The sensitivity of the CIS agrees well with models of the optical delay, given the crystal geometry. While the upper divertor system is currently not stabilized, it will enable comparison of trends in both the “crown” of single null plasmas, and in the upper divertor of double null plasmas. The new periscope optical system is operational, and a temperature-controlled CIS system is currently being installed. A matrix-based inversion routine to calculate the flow velocity image from the phase image has been developed, and is being tested on data; because of efficient computational techniques, several hundred frames (800 by 600 pixels) can be inverted in a few minutes; complete discharges range from 500 to 10,000 frames, depending on signal levels.

Acknowledgment

This work was performed in part under the auspices of the US Department of Energy (US DOE) by LLNL under DE-AC52-07NA27344 and by the US DOE under DE-FC02-04ER54698. DIII-D data shown in this paper can be obtained in digital format by following the links at https://fusion.gat.com/D3D_DMP.

References

[1] Braginskii, S. I., in Reviews of Plasma Physics, edited by Leontovich, M. A. (Consultants Bureau, New York, 1965), Vol. I, p. 205

[2] see for example, Boedo, J. et al Phys. Plasmas **18**, 032510 (2011).

[3] see, for example, Likonen, J. et al Journ. Nucl. Mat. **438**, S42 (2013); Allen, S. L. et al Proc. 23rd IAEA, 2010, Daejeon, Korea.

[4] Groth, M. et al., Proc. 18th PSI, Toledo, Spain (2008), published in J. Nucl. Mat.

[5] Briesemeister, A. R. et al., "Impurity Ion Flow and Temperature Measured in a Detached Divertor with Externally Applied Non-Axisymmetric Fields on DIII-D, these proceedings.

[6] Howard, J. et al Rev. Sci Instrum. 81 (2010) 10E528

[7] Francon, M. and Mallick, S. *Polarization Interferometers*, Wiley-Interscience, 1971, Appendix B, 141.

[8] Tobin, R. Weber, et al J. Nucl. Mater. 438 (2013) S1257

[9] Silburn, et al., "A Coherence Imaging Diagnostic for Plasma Flow Measurements, York Plasma Institute, September 2012.

Figure Captions

Fig. 1. DIII-D cross-section showing location of the three CIS systems. The lower divertor system has precise temperature control and a calibration source located in the shield box; the plasma light is coupled by relay optics. The upper divertor uses an unshielded intensified CID camera. The midplane system is currently being installed.

Fig. 2. Representative phase data from the DIII-D lower divertor flow camera. In the top frame, the raw data image is shown for one time frame with three regions of interest selected. Each image is demodulated, resulting in phase and brightness images. The phase from the three regions (proportional to the inner product of the C2+ velocity vector and the line of sight) is then calculated as a function of time, as shown in the corresponding three panels in the lower frame. The discharge shape changes from lower expanded boundary plasma (EFIT inset at 1000ms) to nearly circular at 2500ms (EFIT inset at 2560ms) – the two plasmas are also overlaid; there is a clear shift in the line-integrated velocities in the three regions of interest from the diverted phase to the circular plasma.

Fig. 3. Top: the relative brightness of the calibration lamp emission lines (right scale) plotted with the transmission (left scale) of the two interference filters. Bottom: The measured sensitivity of the crystal (5.8 mm, 30 degrees our label Claser1) was obtained with these emission lines. As shown in the inset, a 1.5 Å filter was thermally tuned to obtain the rough slope of the sensitivity curve; a high resolution spectrometer simultaneously tracked the central wavelength. The phase change divided by 2π from the interferogram (center of image) for the emission lines is plotted as a function of the fractional change in wavelength $\Delta\lambda/\lambda$. Two interference filters were used to transmit the lines, but block the Ti line at 4667.4 Å. The measured slope is $(\Delta\varphi/2\pi) = 1350 \pm 21\ (\Delta\lambda/\lambda)$, which agrees well with the model [6].

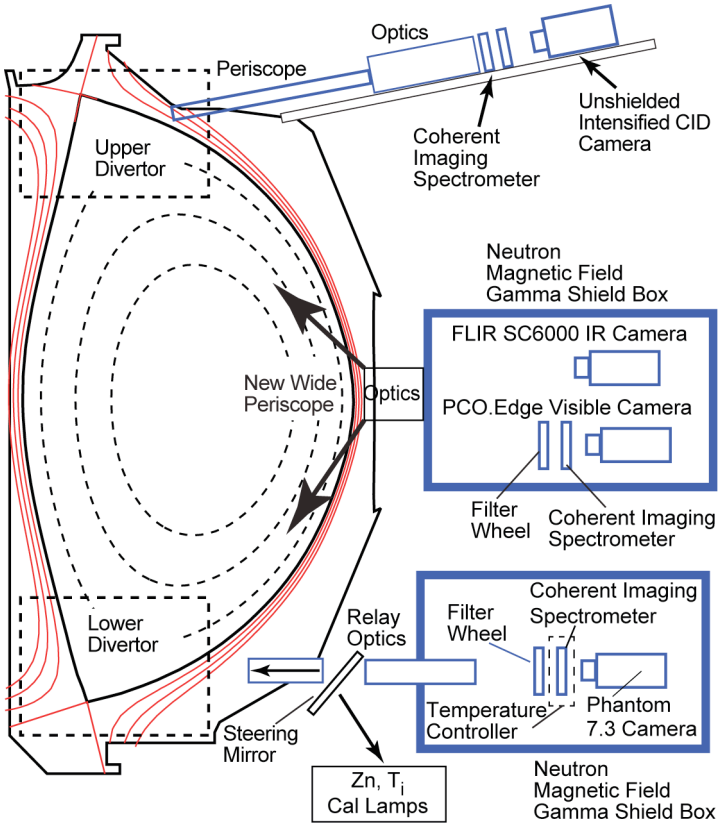
Optics
Periscope
Unshielded
Intensified CID
Camera
Coherent
Imaging
Spectrometer
Upper
Divertor
Neutron
Magnetic Field
Gamma Shield Box
FLIR SC6000 IR Camera
New Wide
Periscope
Optics
PCO.Edge Visible Camera
Filter
Wheel
Coherent Imaging
Spectrometer
Coherent Imaging
Spectrometer
Filter
Wheel
Lower
Divertor
Relay
Optics
Temperature
Controller
Phantom
7.3 Camera
Steering
Mirror
Zn, T_i
Cal Lamps
Neutron
Magnetic Field
Gamma Shield Box

Figure 1

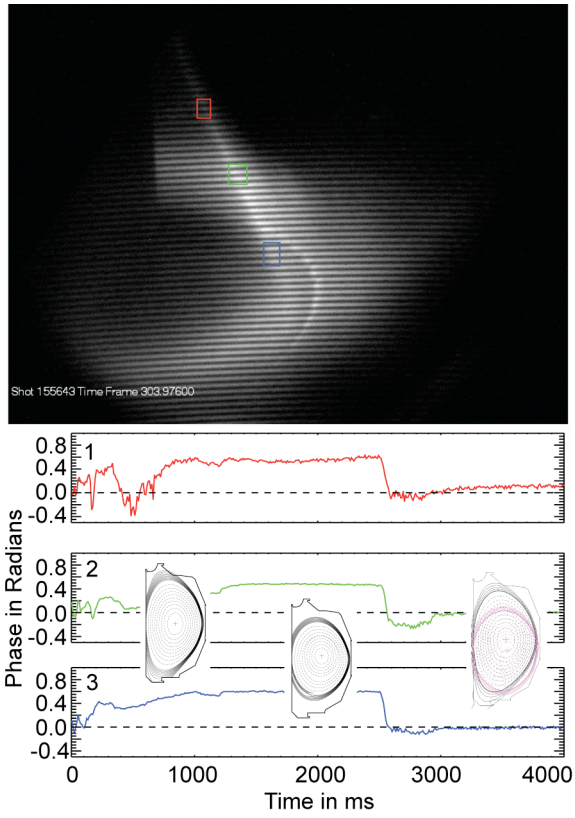
Shot 155643 Time Frame 303.97600
Phase in Radians
0.8
0.4
0.0
-0.4
1
2
3
0
1000
2000
3000
4000
Time in ms

Figure 2

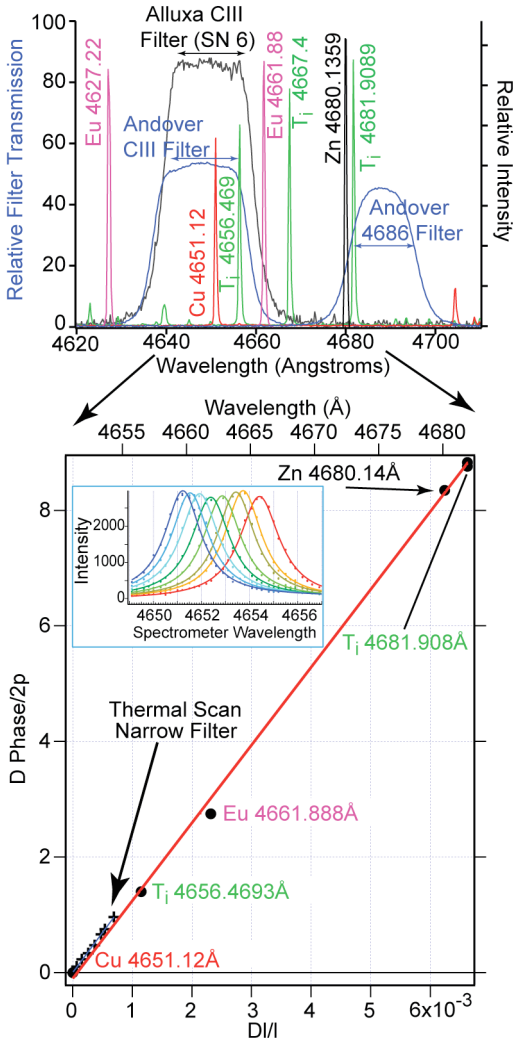
Alluxa CIII
Filter (SN 6)
Eu 4627.22
Andover
CIII Filter
Eu 4661.88
Ti 4667.4
Zn 4680.1359
Ti 4681.9089
Andover
4686 Filter
Cu 4651.12
Ti 4656.469
Relative Filter Transmission
Relative Intensity
Wavelength (Angstroms)
Wavelength (Å)
Zn 4680.14Å
Intensity
Spectrometer Wavelength
Ti 4681.908Å
Thermal Scan
Narrow Filter
Eu 4661.888Å
Ti 4656.4693Å
Cu 4651.12Å
D Phase/2p
DI/I

Figure 3